

SIMILARITY SIGNATURE CURVES FOR FORMING PERIODIC ORBITS IN THE LORENZ SYSTEM

JINDI LI AND YUN YANG*

Dedicated to Professor Peter J. Olver on the occasion of his 70th birthday

ABSTRACT. In this paper, we systematically investigate the short periodic orbits of the Lorenz system by the aid of the similarity signature curve, and a novel method to find the short-period orbits of the Lorenz system is proposed. The similarity invariants are derived by the equivariant moving frame theory and then the similarity signature curve occurs along with them. The similarity signature curve of the Lorenz system presents a more regular behavior than the original one. By combining the sliding window method, the quasi-periodic orbits can be detected numerically, all periodic orbits with period $p \leq 8$ in the Lorenz system are found, and their period lengths and symbol sequences are calculated.

1. INTRODUCTION

The Lorenz system was initially derived from the Oberbeck-Boussinesq approximation by Lorenz in 1963 [23]. Since then, chaos, as an interesting phenomenon in nonlinear dynamical systems has become a widely-studied topic of great interest to specialists and non-specialists alike. Tucker strictly proved the existence of the Lorenz attractor [33], which laid the foundation for subsequent research. In fact, there are infinite periodic orbits in chaotic attractors, and unstable periodic orbits can be used to characterize the chaotic state of the system. Therefore, exploring the existence and position of periodic orbits in chaotic systems attracts the researchers' attention.

In chaos, finding all possible symmetries, i.e., self-equivalences or self-congruences provides an effective way to understand the mathematical properties of the whole system. Generally, the efficient solution of an equivalence problem rests on investigating some related invariants. In fact, invariants supply us with a moduli space of a certain kind of geometric object under group transformations. To obtain the invariants of submanifolds for general transformation groups, Fels and Olver formulated a new, powerful, constructive approach to the equivariant moving frame theory [10]. Let M be a smooth, meaning C^∞ manifold with a sufficiently high order jet bundle, and suppose G is a Lie group acting smoothly on M via prolongation. The practical construction of a moving frame is based on a choice of cross section $K \subset M$ to the group orbits [10, 30]. For example, the right-equivariant moving frame map $\rho : M \rightarrow G$ is locally uniquely obtained by solving the normalization equations $g \cdot z \in K$ for the group parameters $g = \rho(z)$ in terms of the point $z \in M$. Then substituting the moving frame formulae $g = \rho(z)$ into the unnormalized components leads to the fundamental invariants $I_1(z), \dots, I_{m-r}(z)$, where r

* Corresponding author: yangyun@mail.neu.edu.cn

Key words and phrases. Lorenz system; similarity signature curve; periodic orbit; sliding window method.

and m denote the dimensions of G and M , respectively. Then every invariant $I(z)$ can be locally uniquely expressed as a function of the fundamental invariants [29].

According to Cartan's main idea, two regular submanifolds are (locally) equivalent if and only if they have identical syzygies among all their differential invariants. More generally, as a consequence of the Fundamental Basis Theorem [28], one can verify that, for any Lie group action, the entire algebra of differential invariants can be generated from a finite number of low order invariants by repeated invariant differentiation. These typically include the generating differential invariants I^1, I^2, \dots, I^l as well as a certain finite collection of their invariant derivatives I^{ν_j} . These differential invariants serve to define a signature map $\sigma : S \rightarrow \Sigma \subset \mathbb{R}^N$ whose image is a differential invariant signature of the original submanifold S . Under certain regularity assumptions, the signature solves the equivalence problem: two p -dimensional submanifolds are locally equivalent under the transformation group if and only if they have identical signatures [30].

The signature curve $\Sigma \subset \mathbb{R}^2$ of the Euclidean plane curve $C \subset \mathbb{R}^2$ is parametrized by the two lowest order differential invariants [18]

$$\chi : C \rightarrow \Sigma = \left\{ \left(\kappa, \frac{d\kappa}{ds} \right) \right\} \subset \mathbb{R}^2.$$

Similarly, the differential invariant signature for the Euclidean space curve $C \subset \mathbb{R}^3$ is defined by

$$\Sigma = \{(\kappa, \kappa_s, \tau)\} \subset \mathbb{R}^3,$$

where κ and τ are the curvature and torsion of the curve C , respectively.

The above-mentioned two types of the signature curve are invariant to both the translation and rotation of the curve. This concept has received considerable attentions in computer vision, mostly in the issues of object recognition and symmetry detection. Calabi et al. introduced a new paradigm, the differentially invariant signature curve or manifold, for the invariant recognition of visual objects, and discussed various aspects of the numerical computation of signatures and their applications [6]. Boutin gave the signature formulas which are invariant under the action of the Euclidean group and affine group respectively. Another important property of the signature curve is that it is valid for any fine partition of a given curve [3]. Hoff and Olver proposed an automated solution to two-dimensional picture puzzles using the signature curve [17]. Bruckstein and Snaked presented a general framework for skew-symmetric detection, based on invariant planar curve descriptions and successfully applied it to mirror-symmetric polygons distorted by affine and projective viewing transformations [5]. The similarity signature curve is a generalization of the signature curve under similarity transformation, which exhibits invariance to translation, rotation, and scaling. Bruckstein and Netravali generalized the curvature versus arc length representation that is invariant under Euclidean motions to general geometric viewing transformations, such as similarity and affine transformations. Such results can simplify the problem of model-based planar object recognition under partial occlusion to the matching of locally invariant signature functions [4]. Ghorbel et al. completed image reconstruction using the similarity signature curve [15]. As a matter of fact, the Lorenz attractor exhibits fractal structure and self-similarity, and simpler structures can be modeled using the similarity signature curve.

Periodic orbit theory is a powerful tool for analyzing the dynamic behavior of chaotic systems, which can effectively calculate the average value of physical quantities of dynamic systems [2, 1]. Many methods for finding periodic orbits have been proposed. The interval method provides a simple computational test for the uniqueness, existence, and nonexistence of the zeros of a map within a given interval vector [20], and supplies research support for the possibility of complete analysis of piecewise continuous systems by combination with the Poincaré map [12]. Galias and Zgliczyński introduced the Krawczyk operator to prove the existence of periodic orbits of infinite-dimensional discrete dynamical systems and found all periodic orbits of a given period [14]. In addition, the traditional approach is to find periodic orbits by a general technique based on the construction of a graph describing the dynamics of the system. Galias and Tucker successfully studied the existence of periodic orbits for a particular type of system by using symbolic dynamics combined with the interval method [13]. Moreover, a variational principle was utilized to determine the periodic orbits of a class of continuous systems and unstable spatiotemporally periodic solutions of extended systems, such as the Rössler attractor [11].

It has also been suggested that it is difficult to obtain an efficient set of Poincaré sections when finding the periodic orbits of turbulent or high-dimensional flows. In response to this situation, some people proposed the variational method. Lan replaced the Poincaré section with the variational method and verified the existence of periodic orbits in the numerical calculation [21].

In this paper, we present a method that can be employed to model periodic orbits of the Lorenz system, which relies on the similarity signature curve of the system, the interval method, and the sliding window method. The similarity signature curve of the system is calculated, and then the trajectory of the Lorenz system is segmented by the sliding window method. Each quasi-periodic orbit is verified by using the Krawczyk operator. This makes it possible to find periodic orbits in the trajectories between the segmentation points.

The structure of this paper is as follows. In Sec.2, we introduce the Lorenz equation which sketches the chaotic behavior, together with the typical parameters. On the other hand, the similarity invariants are derived by using the equivariant moving frame theory, and the similarity signature curve of the Lorenz attractor is described. In Sec. 3, the sliding window method is improved, and the algorithm based on the similarity signature curve to segment trajectories is proposed, which can obtain the sequence of segmentation points. The trajectories between these points form quasi-periodic orbits. In Sec. 4, all periodic orbits with period $p \leq 8$ in the Lorenz system are shown, and the period number, period length, and motion trajectory of each periodic orbit are listed. The results of this paper are summarized in Sec. 5.

Acknowledgements. This work was supported by the Fundamental Research Funds for the Central Universities under grant-N2104007, and the second author would also like to express his deep gratitude to Professor Peter J. Olver for his encouragement and help during his stay in School of Mathematics, University of Minnesota as a Visiting Professor, while part of this work was completed.

2. LORENZ SYSTEM AND ITS SIMILARITY SIGNATURE CURVE

2.1. Lorenz system dynamics.

The Lorenz system, as the benchmark system for chaotic dynamics, is the first chaotic dissipative system discovered in numerical experiments. In this section, we discuss the relationship between the similarity signature curve and the periodic orbit. In details, the Lorenz equations can be described as a system of three differential equations, namely,

$$\begin{cases} \dot{x}(t) = \sigma(y(t) - x(t)), \\ \dot{y}(t) = rx(t) - y(t) - x(t)z(t), \\ \dot{z}(t) = x(t)y(t) - \eta z(t), \end{cases}$$

where \dot{x} denotes the derivative of x with respect to time t . The positive parameters σ , η , and r raise up from the physical context and Lorenz chose in his original work

$$\sigma = 10, \quad \eta = \frac{8}{3}, \quad r = 28.$$

In this paper, we consider the numerical simulation of the Lorenz system with above parameter values. Fig. 1 shows a numerical approximation with the help of the computer software Matlab.

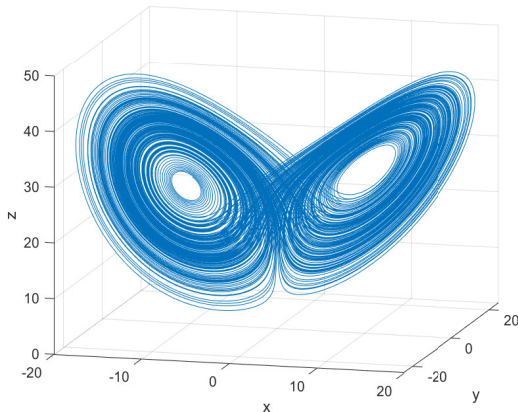


FIGURE 1. A trajectory of the Lorenz system.

First of all, the Lorenz equations contain symmetry. Applying the coordinate transformation

$$(x, y, z) \rightarrow (-x, -y, z),$$

the equations remain the same.

For $r < 1$ (and σ, η arbitrarily), the point $(0, 0, 0)$ is the only fixed point, which is automatically asymptotic stable. It holds that all solutions converge to the origin as $t \rightarrow \infty$. At $r = 1$, it occurs a supercritical Pitchfork-bifurcation and two new fixed points appear. They fulfill

$$x = y = \sqrt{b(r-1)}, \quad z = r - 1.$$

When $r > r_H \approx 24.737$, the Lorenz system, which exhibits chaotic behavior, is the object of our study.

In addition, its stability matrix can be obtained from the Lorenz equations

$$M = \begin{bmatrix} -\sigma & \sigma & 0 \\ r - z_0 & -1 & -x_0 \\ y_0 & x_0 & -\eta \end{bmatrix},$$

where x_0 , y_0 , and z_0 are the coordinates of the stable points. The eigenvalues at stable points indirectly describe the degree to which trajectories in its vicinity are attracted or repelled. The eigenvalue at the origin is $(\lambda^{(1)}, \lambda^{(2)}, \lambda^{(3)}) = (11.83, -2.67, -22.83)$, and the eigenvalues at the other two symmetrical stable points are $(\mu^{(1)} \pm \omega^{(1)}i, \lambda^{(3)}) = (0.094 \pm 10.19i, -13.85)$. The unstable eigenplane of the origin is spanned by $\text{Re } e^{(1)}$ and $\text{Im } e^{(1)}$. The Lorenz flow has an unstable eigenvector $e^{(1)}$ and two stable eigenvectors $e^{(2)}$, $e^{(3)}$ near the origin.

In [8], the motion of the Lorenz attractor is given in numerical terms. The periodic time scale in the neighborhood of the equilibrium $(x, y, z) = (0, 0, 0)$ is of order $\approx T$. The contraction/expansion radially by the multiplier Λ_{radial} , and by the multiplier Λ_j along the $e^{(j)}$ eigen-direction per a turn of the spiral:

$$T = 2\pi/\omega, \quad \Lambda_{radial} = e^{T\mu}, \quad \Lambda_j = e^{T\mu^{(j)}}.$$

The trajectory period around the critical point is about $T = 2\pi/10.19 \approx 0.62s$. Near the two stable points the unstable manifold trajectories spiral out, with very small radial per-turn expansion multiplier $\Lambda^1 = \exp(0.094T) \approx 1.06$, and very strong contraction multiplier $\Lambda^3 = \exp(-13.85T) \approx 1.957 \times 10^{-4}$ onto the unstable manifold. This contraction confines the Lorenz attractor to a two-dimensional surface. In the neighborhood of the origin, the trajectories have an extremely strong contraction along the $e^{(3)}$ direction and the slowest contraction along the $e^{(2)}$ direction. In the plane, the expansion of the attractor in the $e^{(1)}$ direction takes precedence over the contraction in the $e^{(2)}$ direction, which makes it difficult for a few trajectories can approach the origin.

2.2. Similarity signature curve.

The goal of this part is to establish a basic functional relation or syzygy among the differential invariants under the action of the similarity group $\text{Sim}(3) = \{\lambda Ax + b\}$, where A is a real orthogonal 3×3 matrix, $b \in \mathbb{R}^3$ is a real vector and $\lambda > 0$ is a real number. In fact, the similarity invariants have been obtained in [7, 9]. Here we mainly use the equivariant moving frame theory to build the syzygy and the similarity signature curve.

We denote points in \mathbb{R}^3 by $z = (x, u, v) \in \mathbb{R}^3$, with $z(t) = (x(t), u(t), v(t))$ for $t \in I \subset \mathbb{R}$ being a smoothly parametrized curve.

Let us consider the action

$$(X, U, V) = Z = g \cdot z = g \cdot (x, u, v)$$

of the similarity group $\text{Sim}(3)$ in \mathbb{R}^3 , so that

$$(2.1) \quad X = k\alpha \cdot z + a, \quad U = k\beta \cdot z + b, \quad V = k\gamma \cdot z + c,$$

where $k > 0$, a, b, c are real numbers, α, β, γ are the rows of the real orthogonal 3×3 matrix.

To construct a (right) equivariant moving frame, we prolong the $\text{Sim}(3)$ action to the curve jet spaces J^n , which has local coordinates

$$z^{(n)} = (x, u, v, u_x, v_x, u_{xx}, v_{xx}, \dots, u_n, v_n).$$

The formulae for the prolonged action on J^n are provided by implicit differentiation, based on

$$dX = k\alpha \cdot z_t dt, \quad D_X = \frac{1}{k\alpha \cdot z_t} \frac{d}{dt}.$$

Then we have

$$\begin{aligned} U_X &= \frac{\beta \cdot z_t}{\alpha \cdot z_t}, & V_X &= \frac{\gamma \cdot z_t}{\alpha \cdot z_t}, \\ U_{XX} &= \frac{(\alpha \cdot z_t)(\beta \cdot z_{tt}) - (\alpha \cdot z_{tt})(\beta \cdot z_t)}{k(\alpha \cdot z_t)^3}, \\ V_{XX} &= \frac{(\alpha \cdot z_t)(\gamma \cdot z_{tt}) - (\alpha \cdot z_{tt})(\gamma \cdot z_t)}{k(\alpha \cdot z_t)^3}. \end{aligned}$$

To compute the equivariant moving frame, we must normalize the $\dim\{\text{Sim}(3)\} = 7$ independent group parameters by setting 7 of the transformed jet variables equal to conveniently chosen constants. This corresponds to the choice of a cross section to the prolonged group orbits, or, equivalently, to placing the curve in normal form, [28]. The standard cross section that produces the classical moving frame is given by

$$x = u = v = u_x = v_x = v_{xx} = 0, \quad u_{xx} = 1.$$

The determination of the moving frame associated with the above cross-section relies on solving the corresponding normalization equations

$$X = U = V = U_X = V_X = V_{XX} = 0, \quad U_{XX} = 1,$$

for the group parameters $g \in \text{Sim}(3)$, using the explicit formulas for the prolonged Euclidean transformations that were obtained by implicit differentiation.

The order zero normalizations $X = U = V = 0$ prescribe the translation parameters of the group element $g \in \text{Sim}(3)$. Since they play no further role in the prolonged action or other moving frame formulae, we can effectively ignore them from here on. After some obvious simplification, we find

$$\beta \cdot z_t = 0, \quad \gamma \cdot z_t = 0, \quad \gamma \cdot z_{tt} = 0, \quad \frac{\beta \cdot z_{tt}}{k(\alpha \cdot z_t)^2} = 1.$$

We impose the nondegeneracy condition $|z_t \wedge z_{tt}| \neq 0$. Therefore, the right-equivariant moving frame induced by the cross-section is given by

$$(2.2) \quad \begin{aligned} \gamma &= \frac{z_t \wedge z_{tt}}{|z_t \wedge z_{tt}|}, & \beta &= \frac{|z_t|^2 z_{tt} - (z_t \cdot z_{tt})z_t}{\||z_t|^2 z_{tt} - (z_t \cdot z_{tt})z_t\|} = \frac{|z_t|^2 z_{tt} - (z_t \cdot z_{tt})z_t}{|z_t| |z_t \wedge z_{tt}|}, \\ \alpha &= \beta \wedge \gamma = \frac{z_t}{|z_t|}, & k &= \frac{\beta \cdot z_{tt}}{(\alpha \cdot z_t)^2} = \frac{|z_t \wedge z_{tt}|}{|z_t|^3}. \end{aligned}$$

As always, a complete system of functionally independent differential invariants is obtained by invariantization, that is, substituting the moving frame formulae into the unnormalized transformation rules. All other differential invariants are obtained by differentiating the curvature and torsion with respect to the similarity length element,

$$d\tilde{s} = \frac{|z_t \wedge z_{tt}|}{|z_t|^2} dt,$$

which comes from substituting the moving frame formula for α and k into dX .

$$U_{XXX} = \frac{1}{k^2 (\alpha \cdot z_t)^5} \times \left((\beta \cdot z_{ttt})(\alpha \cdot z_t)^2 \right. \\ \left. - (\beta \cdot z_t)(\alpha \cdot z_t)(\alpha \cdot z_{ttt}) - 3(\alpha \cdot z_{tt})(\beta \cdot z_{tt})(\alpha \cdot z_t) + 3(\alpha \cdot z_{tt})^2(\beta \cdot z_t) \right), \\ V_{XXX} = \frac{1}{k^2 (\alpha \cdot z_t)^5} \times \left((\gamma \cdot z_{ttt})(\alpha \cdot z_t)^2 \right. \\ \left. - (\gamma \cdot z_t)(\alpha \cdot z_t)(\alpha \cdot z_{ttt}) - 3(\alpha \cdot z_{tt})(\gamma \cdot z_{tt})(\alpha \cdot z_t) + 3(\alpha \cdot z_{tt})^2(\gamma \cdot z_t) \right).$$

The generating differential invariants are the similarity curvature $\tilde{\kappa}$, obtained from u_{xxx} , and the similarity torsion $\tilde{\tau}$, obtained from v_{xxx} . By using (2.2), a short computation produces the required expressions for the curvature and torsion invariants

$$\tilde{\kappa} = \iota(u_{xxx}) = \frac{(z_t \wedge z_{ttt}) \cdot (z_t \wedge z_{tt}) |z_t|^2 - 3(z_t \cdot z_{tt}) |z_t \wedge z_{tt}|^2}{|z_t \wedge z_{tt}|^3}, \\ \tilde{\tau} = \iota(v_{xxx}) = \frac{|z_t|^3 [z_t, z_{tt}, z_{ttt}]}{|z_t \wedge z_{tt}|^3}.$$

Remark 2.1. In fact, taking $k = 1$ in (2.1) and using cross section $x = u = v = u_x = v_x = v_{xx} = 0$, a similar process yields the Euclidean arc element $ds = |z_t| dt$, the Euclidean curvature $\kappa = \iota(u_{xxx}) = \frac{|z_t \wedge z_{tt}|}{|z_t|^3}$ and the Euclidean torsion $\tau = \iota(v_{xxx})/\kappa = \frac{[z_t, z_{tt}, z_{ttt}]}{|z_t \wedge z_{tt}|^2}$. At the same time, $\iota(u_{xxx}) = \kappa_s$.

By using the inductive construction method of moving frames introduced by Kogan [19], we can see $\text{Sim}(3) = B \cdot \text{SE}(3)$, where $B = \begin{pmatrix} k & 0 & 0 \\ 0 & k & 0 \\ 0 & 0 & k \end{pmatrix}$ and $B \cap \text{SE}(3) = \{I, -I\}$ is finite. Now we prolong the action of B up to third order

$$x \rightarrow kx, \quad u \rightarrow ku, \quad v \rightarrow kv, \quad u_x \rightarrow u_x, \quad v_x \rightarrow v_x, \\ u_{xx} \rightarrow \frac{u_{xx}}{k}, \quad v_{xx} \rightarrow \frac{v_{xx}}{k}, \quad u_{xxx} \rightarrow \frac{u_{xxx}}{k^2}, \quad v_{xxx} \rightarrow \frac{v_{xxx}}{k^2}.$$

Restricting these transformations to the Euclidean cross section $K_E = \{x = u = v = u_x = v_x = v_{xx} = 0\}$, we obtain

$$u_{xx} \rightarrow \frac{u_{xx}}{k}, \quad u_{xxx} \rightarrow \frac{u_{xxx}}{k^2}, \quad v_{xxx} \rightarrow \frac{v_{xxx}}{k^2}.$$

The above action is free on the open subset $\{z \in K_E | u_{xx} \neq 0\}$, and we choose the cross section $K = \{z \in K_E | u_{xx} = 1\}$ to the orbits of B on K_E . This produces a moving frame $\rho_B : K_E \rightarrow B$, that is,

$$k = u_{xx}.$$

Thus we obtain the expression of the similarity invariants $\tilde{\kappa}$ and $\tilde{\tau}$ in terms of Euclidean invariants

$$\tilde{\kappa} = \frac{\kappa_s}{\kappa^2}, \quad \tilde{\tau} = \frac{\tau}{\kappa}.$$

Let us introduce the following basis for the infinitesimal generators in the Lie algebra of $\text{Sim}(3)$

$$\begin{aligned}\mathbf{v}_1 &= \partial_x, & \mathbf{v}_2 &= \partial_u, & \mathbf{v}_3 &= \partial_v, & \mathbf{v}_4 &= v\partial_u - u\partial_v, \\ \mathbf{v}_5 &= -u\partial_x + x\partial_u, & \mathbf{v}_6 &= -v\partial_x + x\partial_v, & \mathbf{v}_7 &= x\partial_x + u\partial_u + v\partial_v.\end{aligned}$$

The prolonged infinitesimal generators of the group $\text{Sim}(3)$ action on curve jets are

$$\begin{aligned}\text{prv}_1 &= \partial_x, & \text{prv}_2 &= \partial_u, & \text{prv}_3 &= \partial_v, \\ \text{prv}_4 &= v\partial_u - u\partial_v + v_x\partial_{u_x} - u_x\partial_{v_x} + v_{xx}\partial_{u_{xx}} - u_{xx}\partial_{v_{xx}} + \cdots, \\ \text{prv}_5 &= -u\partial_x + x\partial_u + (1 + u_x^2)\partial_{u_x} + u_x v_x \partial_{v_x} + 3u_x u_{xx} \partial_{u_{xx}} \\ &\quad + (u_{xx}v_x + 2u_x v_{xx})\partial_{v_{xx}} + (3u_{xx}^2 + 4u_x u_{xxx})\partial_{u_{xxx}} \\ &\quad + (u_{xxx}v_x + 3u_{xx}v_{xx} + 3u_x v_{xxx})\partial_{v_{xxx}} + \cdots, \\ \text{prv}_6 &= -v\partial_x + x\partial_v + v_x u_x \partial_{u_x} + (1 + v_x^2)\partial_{v_x} + (v_{xx}u_x + 2v_x u_{xx})\partial_{u_{xx}} \\ &\quad + 3v_x v_{xx} \partial_{v_{xx}} + (v_{xxx}u_x + 3v_{xx}u_{xx} + 3v_x u_{xxx})\partial_{u_{xxx}} \\ &\quad + (3v_{xx}^2 + 4v_x v_{xxx})\partial_{v_{xxx}} + \cdots, \\ \text{prv}_7 &= x\partial_x + u\partial_u + v\partial_v - u_{xx}\partial_{u_{xx}} - v_{xx}\partial_{v_{xx}} - 2u_{xxx}\partial_{u_{xxx}} - 2v_{xxx}\partial_{v_{xxx}} + \cdots.\end{aligned}$$

The invariant arc length derivative $\mathcal{D} = \iota(D_x)$ of any differential invariant $I = \iota(F)$ obtained by invariantizing a differential function F is specified by the recurrence relation

$$(2.3) \quad \mathcal{D}I = \mathcal{D}\iota(F) = \iota(D_x F) + \sum_{i=1}^7 R^i \iota(\text{prv}_i(F)),$$

where R^1, R^2, \dots, R^7 are the Maurer-Cartan invariants. To determine their formulas, we write out (2.3) for the seven phantom invariants which come from the cross section variables $x, u, v, u_x, v_x, u_{xx}, v_{xx}$

$$\begin{aligned}0 = \mathcal{D}\iota(x) &= \iota(1) + R^1, & 0 = \mathcal{D}\iota(u) &= R^2, & 0 = \mathcal{D}\iota(v) &= R^3, & 0 = \mathcal{D}\iota(u_x) &= 1 + R^5, \\ 0 = \mathcal{D}\iota(v_x) &= R^6, & 0 = \mathcal{D}\iota(u_{xx}) &= \tilde{\kappa} - R^7, & 0 = \mathcal{D}\iota(v_{xx}) &= \tilde{\tau} - R^4.\end{aligned}$$

Thus, the general recurrence relation (2.3) becomes

$$\mathcal{D}\iota(F) = \iota(D_x F) - \iota(\text{prv}_1(F)) + \tilde{\tau}\iota(\text{prv}_4(F)) - \iota(\text{prv}_5(F)) + \tilde{\kappa}\iota(\text{prv}_7(F)).$$

Then it is obvious that

$$\iota(u_{xxxx}) = \tilde{\kappa}\tilde{s} + 3 + 2\tilde{\kappa}^2 - \tilde{\tau}^2, \quad \iota(v_{xxxx}) = \tilde{\tau}\tilde{s} + 3\tilde{\kappa}\tilde{\tau}.$$

Definition 2.2. The differential invariant signature for the similarity space curve $C \subset \mathbb{R}^3$ is parametrized by the three lowest order differential invariants

$$\Sigma = \{(\tilde{\kappa}, \tilde{\kappa}\tilde{s}, \tilde{\tau})\} \subset \mathbb{R}^3,$$

where \tilde{s} is the similarity arc length parameter, $\tilde{\kappa}$ and $\tilde{\tau}$ are the similarity curvature and torsion of the curve C , respectively.

In the actual calculation, the curve is composed of discrete points distributed in space. In [6], the authors provided an approach to the numerical approximation of differential invariants, based on a suitable combination of invariants of the group action to compute differential invariant signatures numerically in a fully group-invariant manner. In Fig. 2, suppose P_{i-1}, P_i, P_{i+1} , and P_{i+2} are four successive

points on a three-dimensional curve C . The Euclidean distance between points P_i and P_j is $\text{dist}(P_i, P_j)$. Let

$$\begin{aligned} a &= \text{dist}(P_{i-1}, P_i), & b &= \text{dist}(P_i, P_{i+1}), & c &= \text{dist}(P_{i-1}, P_{i+1}), \\ d &= \text{dist}(P_{i+1}, P_{i+2}), & e &= \text{dist}(P_i, P_{i+2}), & f &= \text{dist}(P_{i-1}, P_{i+2}). \end{aligned}$$

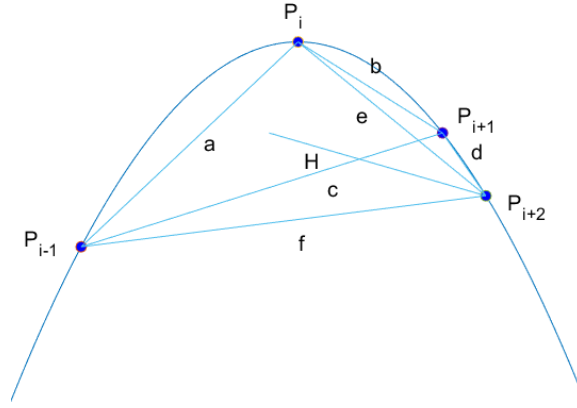


FIGURE 2. Consecutive points for signature approximations.

The equations used to approximate the signature are as follows:

$$\kappa(P_i) = \frac{4\Delta}{abc}, \quad \kappa_s(P_i) = \frac{3(\kappa(P_{i+1}) - \kappa(P_i))}{a + b + c}, \quad \tau(P_i) = \frac{6H}{def\kappa(P_i)},$$

where Δ is the area of the triangle with sides a, b, c , and H is the height of the tetrahedron with sides a, b, c, d, e , and f [18].

2.3. Analysis of the similarity signature curve for the Lorenz attractor.

Compared with the Euclidean signature curve, the similarity signature curve is not only invariant to translation and rotation but also invariant to scale invariance. Fig. 3 and Fig. 4 are the projections of the signature curve and the similarity signature curve of the Lorenz attractor on three coordinate planes. The similarity signature curve of the Lorenz attractor has a stronger self-similarity, which indirectly describes the geometric structure of the Lorenz attractor and is shown as in Fig. 5.

It is worth noting that multiple curves with a given signature can be constructed. Hickman et al. constructed an example of a non-congruence curve with the same Euclidean signature curve [16, 25]. Therefore, the same consequence may occur in the similarity signature curve of the system. Later, we will use the set method to further explain that for different periodic symbol sequences, their similarity signature curves will not completely coincide.

Due to constraints in each direction, the intrinsic fractal structure and self-similarity of the Lorenz attractor are formed. As the decompositions of all the motion states of the Lorenz attractor, Fig. 6 and Fig. 7 depict two completely different states of the similarity signature curve. One is the stable state, and the

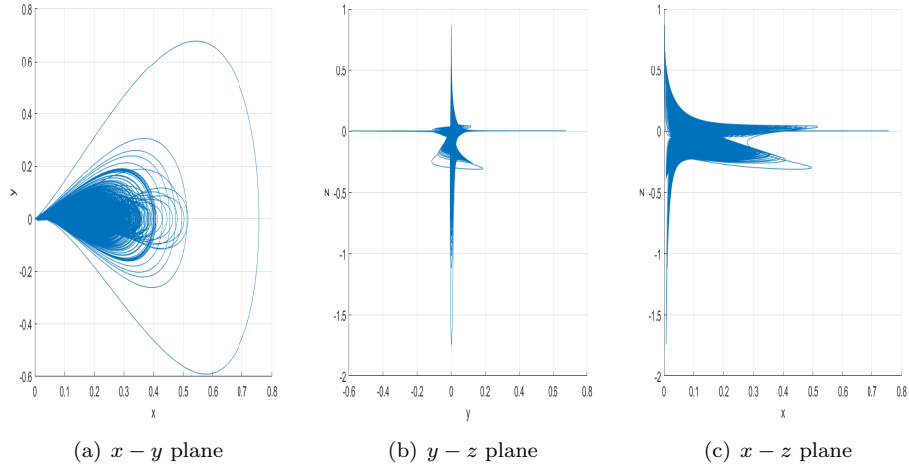


FIGURE 3. Projection of signature curve of Lorenz attractor on coordinate plane.

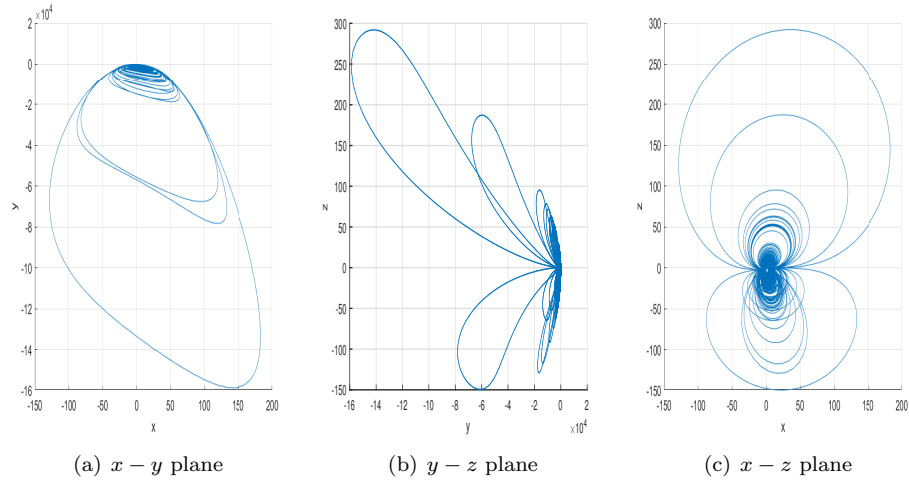


FIGURE 4. Projection of similarity signature curve of Lorenz attractor on coordinate plane.

other is the mutation state. The motion behavior of the Lorenz attractor can be roughly summarized as the random switching of its trajectory between two states. When the similarity signature curve is in a stable state, its corresponding trajectory will continuously rotate around a non-zero stable point. When the state changes, its corresponding trajectory will transition to another non-zero stable point.

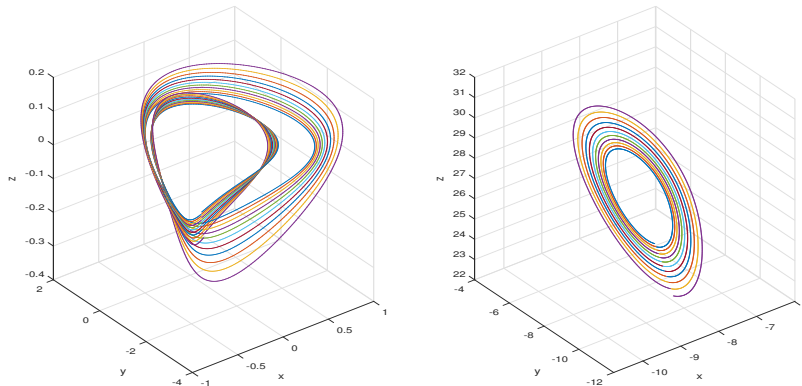


FIGURE 5. The Lorenz attractor with self similarity and its similarity signature curve

3. METHOD OF FINDING PERIODIC ORBITS

The existence of periodic orbits in the Lorenz attractor has been strictly proved [33]. On the basis that the trajectories of the Lorenz system never intersect, we propose a theorem and an algorithm to illustrate the feasibility of using the similarity signature curve to find periodic orbits. The algorithm combines the sliding window method with the similarity signature curve and uses the Krawczyk operator to verify whether there is a real periodic orbit near a quasi-periodic orbit.

3.1. Interval methods.

Interval methods provide simple computational tests for the uniqueness, existence, and nonexistence of zeros of a map within a given interval vector [13]. Simplification of continuous-time systems to discrete systems benefits from the Poincaré map. The Poincaré map reflects the dependence of the successor point on the predecessor point when the trajectory repeatedly crosses the same plane which can simplify the quasi-periodic orbit into a series of discrete points. The Poincaré map for the autonomous system is as follows.

Definition 3.1 ([31]). Let x^* be a point on a limit cycle and let Π be an $(n - 1)$ -dimensional hyperplane transversal to Γ at x^* . The trajectory emanating from x^* will hit Π at x^* in T seconds, where T is the minimum period of the limit cycle. Due to the continuity of ϕ_t with respect to the initial condition, trajectories starting on Π in a sufficiently small neighborhood of x^* will, in approximately T seconds, intersect Π in the vicinity of x^* . Hence, ϕ_t and Π define a mapping P_A of some neighborhood $U \subset \Pi$ of x^* onto another neighborhood $V \subset \Pi$ of x^* . P_A is a Poincaré map of the autonomous system.

The Poincaré map can be simply called as $\Omega : \Pi \rightarrow \Pi$ and it is defined as $\Omega(x) = \varphi(t(x), x)$ where $\Pi = \Pi_1 \cup \dots \cup \Pi_m$ is the union of hyperplanes, and $t(x)$ is the return time after which the trajectory $\varphi(t, x)$ returns to Π . Periodic points of Ω correspond to periodic orbits of the continuous system [13].

A map is constructed to study the existence of period- p orbits of Ω :

$$[F(z)]_k = x^{((k+1) \bmod p)} - \Omega(x^k),$$

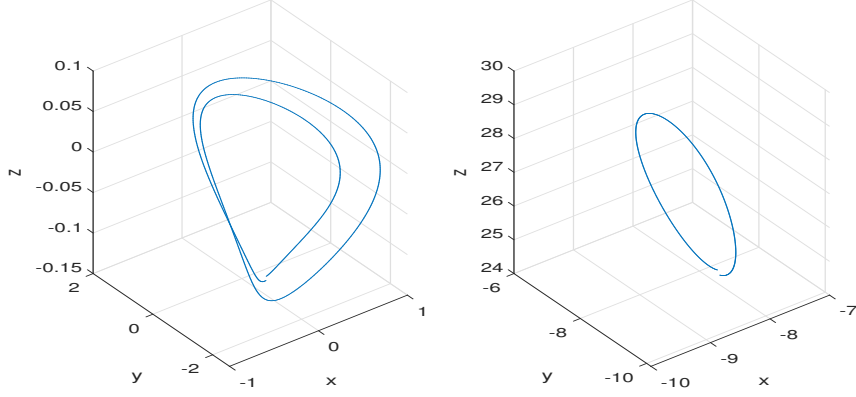


FIGURE 6. Similarity signature curve in stable state and the trajectory of its corresponding the Lorenz attractor.

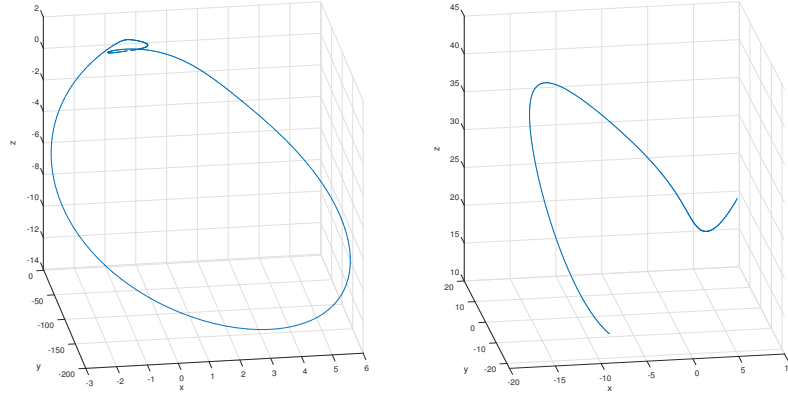


FIGURE 7. Similarity signature curve in mutation state and the trajectory of its corresponding the Lorenz attractor.

where $0 \leq k \leq p$ and $z = (x^{(0)}, x^{(1)}, \dots, x^{(p-1)})$. Zeros of F correspond to period- p points of Ω , i.e., $F(z) = 0$ if and only if $\Omega^p(x^{(0)}) = x^{(0)}$.

The interval method can test the uniqueness, existence, and non-existence of the zeros of the Poincaré map, so it can be used to find the periodic solution of the Lorenz system on the Poincaré section. The Krawczyk operator [20, 26] is:

$$K(\mathbf{z}) = \hat{z} - MF(\hat{z}) - (MF'(\mathbf{z}) - I)(\mathbf{z} - \hat{z}),$$

where $\hat{z} \in \mathbf{z}$, $F(\hat{z})$ is the interval matrix containing the Jacobian matrices $F'(\hat{z})$ for all $z \in \mathbf{z}$, and M is an invertible matrix. Using the method given in [11], the map $\Omega(x)$ and its Jacobian matrix in the Krawczyk operator can be obtained. Generally, we take \hat{z} as the center of \mathbf{z} and M as the inverse of $F'(\hat{z})$. If $\mathbf{z} \cap K(\mathbf{z}) = \phi$, then

there are no period- p orbits in \mathbf{z} . If $K(\mathbf{z}) \subset \text{intz}$, there exists precisely one period- p orbit in \mathbf{z} [21].

3.2. Periodic orbits by the symbolic dynamics based approach.

The following theorem guarantees the feasibility of the algorithm proposed in this paper.

Theorem 3.2. *For two different periodic orbits P_1 and P_2 , their periodic symbol sequences are $S_1 = (s_{11}, s_{12}, \dots, s_{1n_1})$, $S_2 = (s_{21}, s_{22}, \dots, s_{2n_2})$, $1 < n_2 < n_1$, and S_2 is a ordered subset of S_1 . The similarity signature curve of P_2 will not completely coincide with the similarity signature curve of P_1 .*

Proof. For a given periodic symbol sequence $S_0 = (s_0, s_1, \dots, s_{p-1})$, there exists at most one point $x \in N$ with the symbol sequence S such that $R^p(x) = x$ [32]. Then periodic orbits with the same sequence of periodic symbols will not be strictly similar. If the long periodic orbits do not contain short periodic orbits, it means that there will be no periodic orbit with period symbol S_2 in the long period orbit, so this theorem is correct. Otherwise, we will face the following two cases.

(1) P_1 starts with P_2 or ends with P_2 , that is, $S_1 = (S_2, s_{n_2+1}, \dots, s_{n_1})$ or $S_1 = (s_{11}, \dots, s_{n_1-n_2}, S_2)$. For the given S_2 , there exists at most one point $x \in N$ with the symbol sequence S_2 such that $R^{n_2}(x) = x$. The point x exists in the trajectory satisfying the periodic symbol sequence and belongs to the intersection of attractor and trapping region N , then x also satisfies $R^{n_1}(x) = x$. The part of S_1 excluding S_2 can be regarded as a whole, which is called S_3 , that is, $S_1 = (S_2, S_3)$ or $S_1 = (S_3, S_2)$. S_3 is also a sequence of periodic symbols, where $S_3 = (s_{n_2+1}, \dots, s_{n_1})$ or $S_3 = (s_{11}, \dots, s_{n_1-n_2})$.

(2) P_2 is included in P_1 , that is, $S_1 = (s_{11}, \dots, s_{1k}, S_2, k + n_2 + 1, \dots, s_{n_1})$, and then the proof process is similar as the above case. \square

In [32], it was established that there existed a finite set of rectangles $N = N^- \cup N^+ \subset \Pi$ such that N is mapped into itself by the return map $R : \Pi \rightarrow \Pi$. They formed the forward invariant set $\mathcal{A} = \bigcap_{k=0}^{\infty} P^k(N)$. In fact, \mathcal{A} is the intersection of the Lorenz attractor with N . For a trajectory $\{x_n\}_{n=0}^{\infty} \subset N$ where $x_{n+1} = R(x_n)$. Suppose that x' is the similarity signature of x , and we need at least 4 points to approximate x' . The points in the Lorenz attractor will not intersect. According to the continuity of the Lorenz system, we know that the similarity signature curve of the Lorenz attractor is also continuous. When point x satisfies the condition $R^p(x) = x$, the similarity signature of x is also invariant, so there is an invariant set in the similarity signature of the Lorenz attractor. The similarity signature at this point also exists and is unique, otherwise, there will be conflicts.

3.3. Sliding window method based on similarity signature curve.

The sliding window method can solve the problems of finding the properties, such as the length, of a continuous interval that satisfies certain conditions. All trajectories of the Lorenz attractor are processed successively by its similarity signature curve and sliding window method, and the segmented fragments have obvious self-similarity, which is a manifestation of the fractal structure of the Lorenz attractor. It is wise to construct a real periodic orbit based on a quasi-periodic orbit but the initial value of the system limits its accuracy. Experiments show that in the process of finding quasi-periodic orbits, the choice of initial point will affect the final result. A suitable initial point can ensure that the quasi-periodic orbits are similarly

positioned in the Lorenz system. In addition to the initial point, the appropriate window size can more intuitively reflect the relationship between the properties of the data in each window, which is helpful for the division of periodic orbits. The algorithm for finding the periodic orbits of the Lorenz system is implemented according to the rules proposed above.

The algorithm simplifies the problem of finding the periodic orbits of the Lorenz system into the search and combination of two different states of the trajectory. For purposes of clarity, we generate the following pseudo-code and algorithm structure.

Algorithm 1 Sliding window method

Input: The Lorenz system dataset D ; Window size W ; Initial point $P_{1,1}$

Output: Periodic orbit segmentation points z

```

1: Initialize  $z = [P_{1,1}]$ ,  $poi = 0$ ,  $i = 1$ ;
2: Compute  $\tilde{\kappa}$ ,  $\tilde{\kappa}_{\bar{s}}$  and  $\tilde{\tau}$  of the Lorenz system;
3: while  $poi + W \leq \text{length}(D)$  do
4:   for  $j = 1 : W$  do
5:     Compute  $d(j) = \text{dist}(P_{i,1}, P_{i,j})$ ;
6:     Compute  $[val, index] = \min d(j)$ ;
7:     Compute  $P_{i+1,1} = P_{i,index}$ ;
8:      $z = [z, P_{i+1,1}]$ ;
9:   end for
10:   $poi = poi + index$ ;
11:   $i = i + 1$ ;
12: end while
13: return  $z$ ;

```

The similarity signature curve for the Lorenz systems is acquired through the numerical calculation by using the formulas in Sec. 2. Actually, a proper selections of the initial point and window size for the algorithm can ensure the feasibility of the algorithm. The initial point should satisfy two conditions. (1) The closest point to the initial value of the system. (2) The extreme point of the similarity signature curve in the z -axis direction. These ensure that the segmentation points on the trajectory of the Lorenz attractor are more stable. When the trajectory transitions from rotating around one stable point to another stable point, the period of its similarity signature curve is the longest, so the maximum periodic orbit length of the system should be taken into account in the selection window size. If the window size is too small, a complete period may not exist in the window. Suppose the window size is W which satisfies the condition slightly smaller than the length of two periods of the similarity signature curve. Let $W = 2500$, equates to about 1.25s. If the length of the last remaining data is less than the size of the window, it will not be considered. Suppose that the initial point of each window is p_{i1} ($1 \leq i \leq n$), and the other points in a window period are p_{ij} ($2 \leq j \leq 2500$), where n is equal to the number of windows required in the end. By calculating the distances between all points in the longer trajectory and the fixed initial point, we observe the existence of cycles in their distance image, as shown in Fig. 8. After completing the closest point search for the initial points of the similarity signature curve, the trajectory between these two points is always in the form of two circle-like nests. As the degree of the mutation of the similarity signature curve gradually increases, the amplitude

of the distance map also increases, which means that the Lorenz attractor will transition from a stable state to a mutation state.

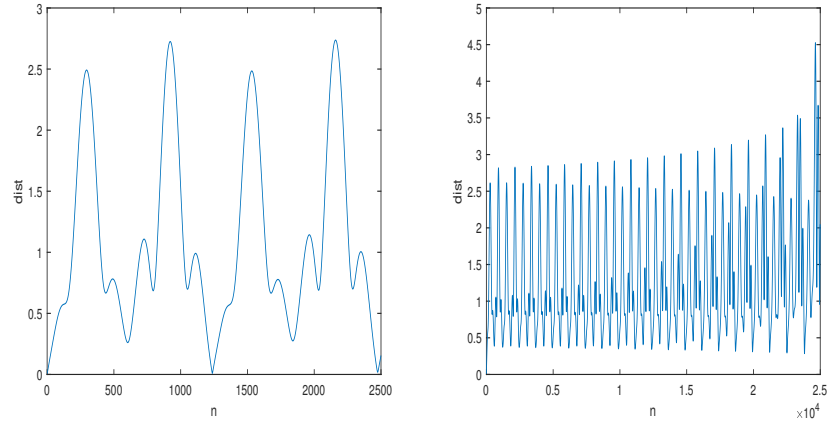


FIGURE 8. Distance between all points in a window and the initial point.

Second, as the trajectory continues to rotate around a non-zero stable point, the point closest to the initial point on each approximate circle in its similarity signature curve gradually moves away from the initial point. As shown in Fig. 9, the distance between them gradually increases. When the point p_{ik} closest to the initial point p_{i1} is found, the initial point needs to be updated. The point p_{ik} will be called the new initial point, and then we recalculate the distance image and update the initial point continuously until the subsequent trajectory ends. Then point p_{ik} is equal to point $p_{i+1,1}$. This part is a detailed explanation of the loop part in the pseudocode.

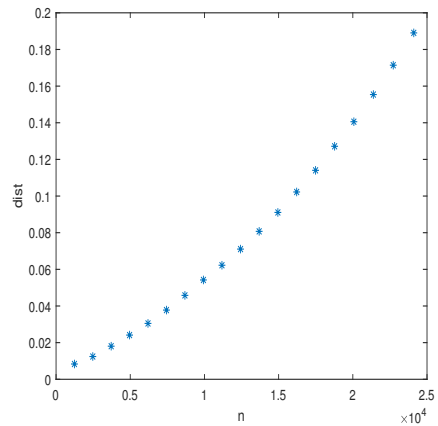


FIGURE 9. The points in the graph represent the distance between the points closest to the starting point in each cycle.

Third, a sequence of points $p = \{p_{11}, p_{21}, \dots, p_{n1}\}$ is obtained by looping, where n is the number of segmentation points and windows required. Filtering segmentation points leaves only points along the same direction of the z -axis. The filtered points form a new point sequence, which is assumed to be $P = \{P_{11}, P_{21}, \dots, P_{k1}\}$, where point P_{i1} is equivalent to point $p_{k1} \in p$. The trajectory between every two points in the point sequence P may be a quasi-periodic orbit. Except for the first and last points in the sequence, the other points are the end of one orbit and the beginning of the next. The endpoints of the quasi-periodic orbits obtained by applying the similarity signature curve can be kept within the neighborhood of 0.0005.

Finally, the periodic orbits are closed. This method is based on the existence of a real periodic orbit in a neighborhood of the quasi-periodic orbit [22]. Table 1 gives the data for quasi-periodic orbits with periods not greater than 5.

In short, there are three advantages of using the similarity signature curve to find periodic orbits: (1) It can reflect the self-similarity of the Lorenz system from the perspective of invariants; (2) High precision is achieved by common methods, which is helpful for quasi-periodic orbits positioning; (3) The order of the periodic orbits is guaranteed and no omission occurs.

TABLE 1. Data of periodic orbits with period $p \leq 5$, including the coordinates of the segmentation points and the distance between the endpoints.

s	x	y	z	dist
LR	-9.727902750	-16.398960521	17.292212679	0.002599810
LLR	-9.836367146	-16.255530452	18.121784817	0.002386087
LLL	-9.835075562	-16.131007675	18.411435859	0.003081481
LLRR	-9.917578308	-15.670162223	19.764832024	0.003614604
LLLLR	-9.918073021	-15.155786811	20.761179930	0.001839419
LLLRR	-9.849285414	-15.553696219	19.723034119	0.002946679
LLRLR	-9.803205079	-16.451041061	17.539781868	0.003687509

3.4. Method summary.

In this method, quasi-periodic orbits are obtained by dividing and recombining the Lorenz attractor by its similarity signature curve. A better approximation of the position of the periodic orbit near the quasi-periodic orbit is found by standard (non-interval) Newton iteration. Finally, the existence of real periodic orbits can be proved by using the Krawczyk operator.

4. PERIODIC ORBITS FOR THE LORENZ SYSTEM

According to the algorithm proposed in the previous section, a sequence $P = (P_{11}, P_{21}, \dots, P_{k1})$ is obtained, where P_{i1} is the point in the Lorenz attractor and is also the starting and ending points of orbits. The standard Newton method contributes to sharpening the approximation and thus obtaining quasi-periodic trajectories. Finally, the Krawczyk operator is used to prove the existence of real periodic

orbits in the neighborhood of their quasi-periodic orbits and all periodic orbits with period $p \leq 8$ are found. The orange part in Fig. 10 is composed of the segmentation points of each periodic orbit. The positions of the segmentation points exhibit similarity due to the invariance to scaling of the similarity signature curve. Each trajectory is labeled in the following ways. Let q be the first intersection of the two-dimensional flow and the return plane Π . When the trajectory intersects the plane to the left of q , it is recorded as L, otherwise, recorded as R. Period- p orbits can be better represented using the sign sequence $S = (s_1, s_2, \dots, s_p)$, for $s_i = L$ or $s_i = R$, for $i = 1, 2, \dots, p$.

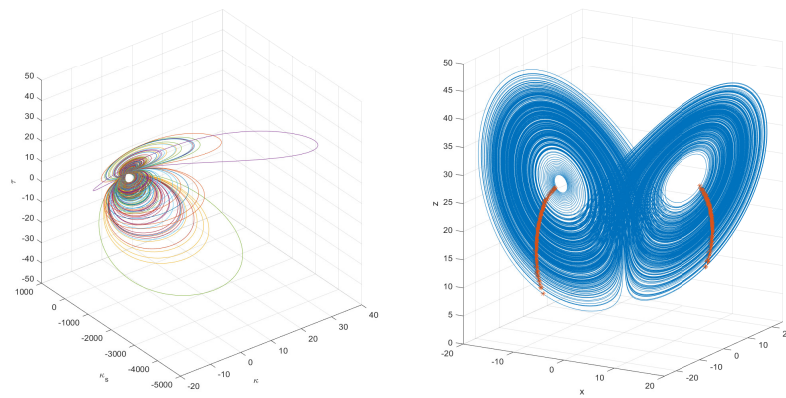


FIGURE 10. Divided similarity signature curve and the positions of the segmentation points on the Lorenz attractor.

There are infinitely long periodic orbits in the Lorenz system, and these long-period orbits can be composed of multiple short-period orbits. Only the coprime periodic orbits are considered when recording periodic orbits. If a sequence is a periodic orbit, only its non-repetitive serial number is recorded as the equivalent form of the periodic orbit.

The one-dimensional symbolic dynamics of the Lorenz system are established to show all the found periodic orbits with periods no greater than 8. We give the period p , the period length T , and the corresponding symbol sequence s for each periodic orbit discovered. The results are reported in Table 2. Fig. 11 illustrates the periodic orbits with period $p \leq 6$. For each pair of symmetric orbits, only periodic orbits with a greater number of L than R are plotted.

5. CONCLUSION

In this paper, a novel method based on the similarity signature curve is proposed for forming the periodic orbits of the Lorenz system, and some experimental results are exhibited to show the efficacy of this method.

Firstly, through the similarity invariants of the Lorenz system and a series of experiments, we can demonstrate the chaotic patterns of the Lorenz system evolution, and ensure the feasibility of the method of applying the similarity signature curve to calculate the periodic orbits.

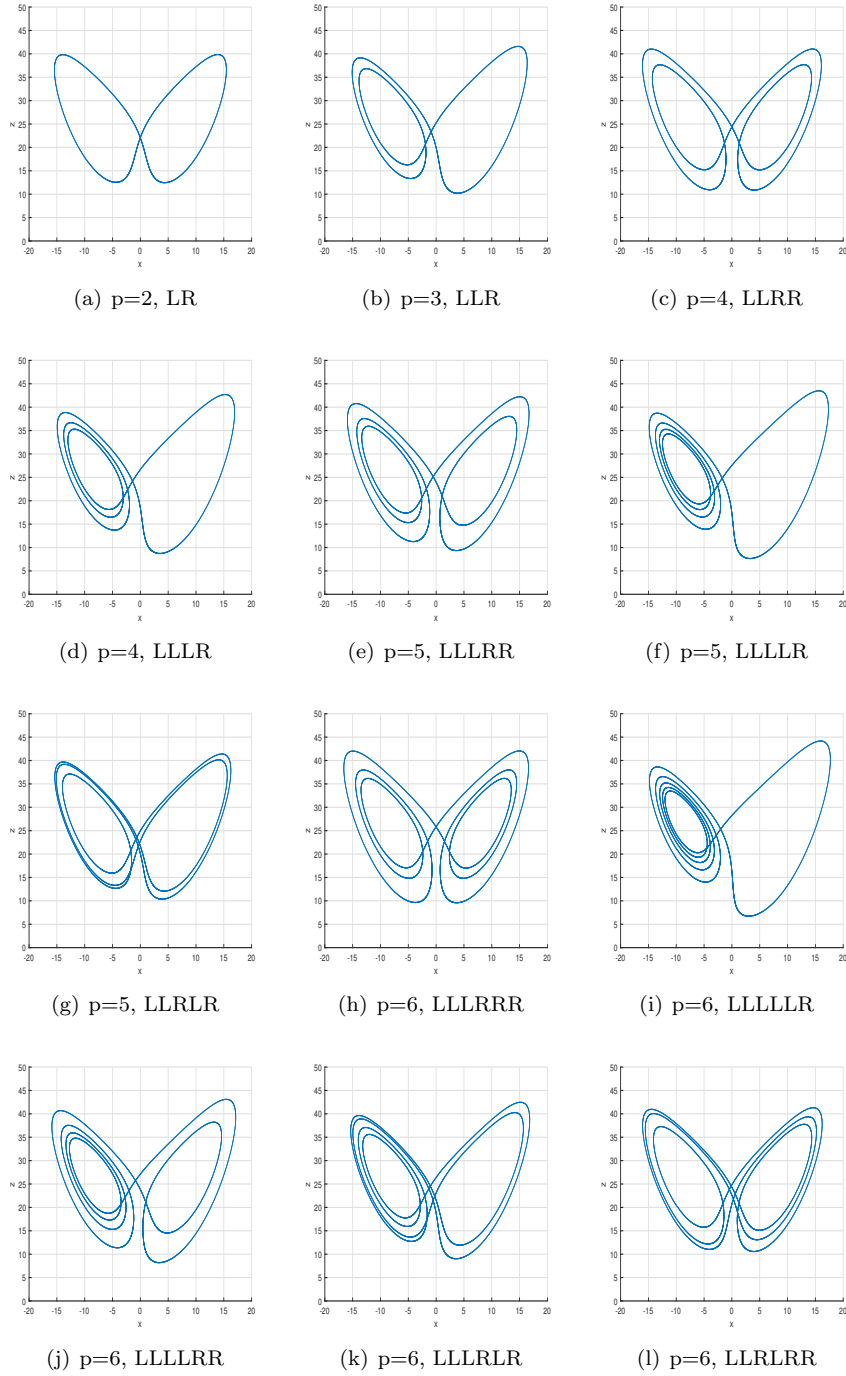


FIGURE 11. Periodic orbits of the Lorenz system with $p \leq 6$, where p is the period, and the order in which L and R appear is the trajectory of the periodic orbit.

TABLE 2. Short periodic orbits, where p is the period of the orbit, T is the flow-time, s is the corresponding symbol sequence.

p	T	s	p	T	s
2	1.55865	LR	7	5.39421	LLRLLRR
3	2.30591	LLR	7	5.42912	LLRLRLR
4	3.02358	LLLRR	8	5.78341	LLLLLLLR
4	3.08428	LLRR	8	5.92499	LLLLLLRR
5	3.72564	LLLLR	8	5.99044	LLLLLRRR
5	3.82025	LLLRR	8	5.99732	LLLLLRLR
5	3.86953	LLRLR	8	6.01003	LLLLRRRR
6	4.41776	LLLLLR	8	6.03523	LLLLRLLR
6	4.53410	LLLLRR	8	6.08235	LLLLRLRR
6	4.56631	LLLRRR	8	6.08382	LLLLRRLR
6	4.59381	LLLRLR	8	6.10805	LLLRLRRR
6	4.63714	LLRLRR	8	6.12145	LLLRLLR
7	5.10303	LLLLLLR	8	6.12233	LLLRLLR
7	5.23419	LLLLLRR	8	6.13512	LLLRRLRR
7	5.28634	LLLLRRR	8	6.15472	LLLRLRLR
7	5.30120	LLLRLR	8	6.17587	LLRLLRLR
7	5.33091	LLLRLR	8	6.18751	LLRLRRLR
7	5.36988	LLLRLRR	8	6.19460	LLRLRLRR
7	5.37052	LLLRLR			

Secondly, in order to continuously obtain the required quasi-periodic orbits, the conditions for the window moving in the sliding window method are improved. The window is updated by repeatedly selecting the points in the subsequent data which are closest to the initial point on the similarity signature curve.

In this way, all periodic orbits with period $p \leq 8$ are found. Also, it is a common fact to predict long-period orbits by using some short-period orbits. However, the longer the period, the larger the error and the more difficult to locate the corresponding position. Searching exact periodic orbits with similarity signature curves offers certain advantages comparing with other methods.

REFERENCES

- [1] ARTUSO R, AURELL E, CVITANOVIC P, Recycling of strange sets: I. Cycle expansions. *Nonlinearity*, **3**, (1990), 325.
- [2] ARTUSO R, AURELL E, CVITANOVIC P, Recycling of strange sets: II. Applications. *Nonlinearity*, **3**, (1990), 361.
- [3] BOUTIN M, Numerically invariant signature curves. *Int J Comput Vision*, **40**, (2000), 235-248.
- [4] BRUCKSTEIN A M, NETRAVALI A N, On differential invariants of planar curves and recognizing partially occluded planar shapes. *Ann Math Artif Intel*, **13**, (1995), 227-250.
- [5] BRUCKSTEIN A M, SNAKED D, Skew symmetry detection via invariant signatures. *Pattern Recogn*, **31**, (1998), 181-192.

- [6] CALABI E, OLVER P J, SHAKIBAN C, TANNENBAUM A, & HAKER S, Differential and Numerically Invariant Signature Curves Applied to Object Recognition. *Int J Comput Vision*, **26**, (1998), 107-135.
- [7] CHOU K S, QU C, Motions of curves in similarity geometries and Burgers-mKdV hierarchies. *Chaos Soliton Fract*, **19**, (2004), 47-53.
- [8] CVITANOVIC P, ARTUSO R, MAINIERI R, TANNER G, VATTAY G, WHELAN N, & WIRZBA A, *Chaos: classical and quantum*. ChaosBook.org (Niels Bohr Institute, Copenhagen 2005), **69**, (2005), 25.
- [9] ENCHEVA R P, GEORGIEV G H, Similar frenet curves. *Results Math*, **55**, (2009), 359-372.
- [10] FELS M, OLVER P J, Moving coframes: II. Regularization and theoretical foundations. *Acta Appl Math*, **55**, (1999), 127-208.
- [11] GALIAS Z, Counting low-period cycles for flows. *Int J Bifurcat Chaos*, **16**, (2006), 2873-2886.
- [12] GALIAS Z, On rigorous study of Poincaré maps defined by piecewise linear systems [electronic circuit example]. *2005 IEEE International Symposium on Circuits and Systems IEEE*, (2005), 3407-3410.
- [13] GALIAS Z, TUCKER W, Validated study of the existence of short cycles for chaotic systems using symbolic dynamics and interval tools. *Int J Bifurcat Chaos*, **21**, (2011), 551-563.
- [14] GALIAS Z, ZGLICZYŃSKI P, Infinite dimensional Krawczyk operator for finding periodic orbits of discrete dynamical systems. *Int J Bifurcat Chaos*, **17**, (2007), 4261-4272.
- [15] GHORBEL F, DERRODE S, MEZHOUD R, BANNOUR T, & DHAHBI S, Image reconstruction from a complete set of similarity invariants extracted from complex moments, *Pattern Recogn Lett*, **27**, (2006), 1361-1369.
- [16] HICKMAN M S, Euclidean signature curves. *J Math Imaging Vis*, **43**, (2012), 206-213.
- [17] HOFF D J, OLVER P J, Automatic Solution of Jigsaw Puzzles. *J Math Imaging Vis*, **49**, (2014), 234-250.
- [18] HOFF D J, OLVER P J, Extensions of invariant signatures for object recognition. *J Math Imaging Vis*, **45**, (2013), 176-285.
- [19] KOGAN I A, Inductive construction of moving frames. *Commun Contemp Math*, **2**, (2002), 53-117.
- [20] KRAWCZYK R, Newton-algorithmen zur bestimmung von nullstellen mit fehler-schranken. *Computing*, **4**, (1969), 187-201.
- [21] LAN Y, CVITANOVIĆ P, Variational method for finding periodic orbits in a general flow. *Phys Rev E*, **69**, (2004), 016217.
- [22] LATHROP D P, KOSTELICH E J, Characterization of an experimental strange attractor by periodic orbits. *Phys Rev A*, **40**, (1989), 4028.
- [23] LORENZ E N, Deterministic nonperiodic flow. *J Atmos Sci*, **20**, (1963), 130-141.
- [24] LÜ J, CHEN G, A new chaotic attractor coined. *Int J Bifurcat Chaos*, **12**, (2002), 659-661.
- [25] MUSSO E, NICOLODI L, Invariant signatures of closed planar curves. *J Math Imaging Vis*, **35**, (2009), 68-85.
- [26] NEUMAIER A, *Interval methods for systems of equations*. Cambridge university press, (1990).
- [27] OLVER P J, *Equivalence, invariants and symmetry*. Cambridge University Press, (1995).
- [28] OLVER P J, Modern developments in the theory and applications of moving frames. *London Math Soc, Impact150 Stories 1*, (2015), 14-50.
- [29] OLVER P J, Moving frames. *J Symb Comput*, **2**, (2002), 53-117.
- [30] OLVER P J, Moving frames and singularities of prolonged group actions. *Selecta Math*, **6**, (2000), 41-77.
- [31] PARKET T S, CHUA L, *Practical numerical algorithms for chaotic systems*. Springer Science & Business Media, (2012).
- [32] TUCKER W, A rigorous ODE solver and Smale's 14th problem. *Found Comput Math*, **2**, (2002), 53-117.
- [33] TUCKER W, The Lorenz attractor exists. *C.R. Acad. Sci. Paris*, **328**, (1999), 1197-1202.

JINDI LI

DEPARTMENT OF MATHEMATICS, NORTHEASTERN UNIVERSITY, SHENYANG, 110819, P.R. CHINA

Email address: lijindi0717@hotmail.com

YUN YANG

DEPARTMENT OF MATHEMATICS, NORTHEASTERN UNIVERSITY, SHENYANG, 110819, P.R. CHINA

Email address: yangyun@mail.neu.edu.cn